Resbee Publishers

Multimedia Research (MR)

Received 18 April, Revised 14 June, Accepted 14 July

Enhanced Crow Search Optimization Algorithm and Hybrid NN-CNN Classifiers for Classification of Land Cover Images

Malige Gangappa
Computer Science Engineering
VNR VignanaJyothi Institute of Engineering and Technology
Hyderabad, Telangana, India
maligegangappa@gmail.com

Kiran Mai C
Computer Science Engineering
VNR VignanaJyothi Institute of Engineering and Technology
Hyderabad, Telangana, India

Sammulal P
Computer Science Engineering
JNTUH College Of Engineering Jagtial (JNTUH CEJ)
Jagtial, Telangana, India

Abstract: The insufficient land cover data contain mainly imperfect the consequence and effects of land cover. Although satellite imaging or remote sensing is used in mapping various spatial and temporal scales, however, its complete endeavor was not hitherto recognized. Therefore, this paper aims to employ a new land cover classification technique by optimal deep learning architecture. Moreover, it comprises three major stages such as segmentation, feature classification, and extraction. At first, the land cover image is segmented and given to the feature extraction process. For feature extraction, VI, like SR, Kauth–Thomas Tasseled Cap and NDVI, are extracted. Moreover, these features are classified by exploiting CNN and NN in both the classifiers, by Enhanced Crow Search Algorithm the number of hidden neurons is optimized. The optimization of hidden neurons is performed so that the classification accuracy must be maximum that is considered as the main contribution.

Keywords: Land Use; CNN; Land Cover Data; NN; Enhanced GWO Algorithm

Nomenclature

Abbreviations	Descriptions
GEOBICA	Geographic Object-Based Image Change Analysis
RCRLBP	Rotated-Corner Local Binary Pattern
VI	Vegetation Index
DCNN	Deep Convolutional Neural Networks
NDVI	Normalized Difference Vegetation Index
RNN	Recurrent Neural Network
FF	Firefly
ResNet	Residual Convolutional Neural Network
SCDAL	Semi-Supervised Center-Based Discriminative Adversarial Learning
UHI	Urban Heat Island
RASTARFM	Robust Adaptive STARFM
FF	Firefly
GA	Genetic Algorithm
FRes	Fine Spatial Resolution
LCZ	Local Climate Zone
PSO	Particle Swarm Optimization
STARFM	Spatial-Temporal Adaptive Reflectance Fusion Model
SAR	Synthetic Aperture Radar
ESTARFM	Enhanced STARFM
SITS	Satellite image time series
SR	Simple Ratio
STITFM	Spatio-Temporal Fusion Model
DCNN	Deep Convolutional Neural Network
ST-MRS	Spatiotemporal Multi-Resolution Segmentation
OBIA	Object-Based Image Analysis
STAARCH	Spatial-Temporal Adaptive Algorithm For Mapping Reflectance Change
Re-ResNet	Recurrent Residual Network
ABC	Artificial Bee Colony
DAP	Dynamic Awareness Probability
LULC	Land Use/Land Cover

1. Introduction

In the past two hundred years, the rapid rise of the human population has resulted in significant adaption in natural environments. The major part of the world's population at present lives in urban areas, a move from the last while people essentially lived in rural regions. Urban regions do not merely adjust the natural environment, but also they have put back they further affect the welfare of the population living within them. Hence, observing urban land employ and land cover change is significant [1].

For dynamic management and planning, monitoring, and the sensible advancement of land, the land use/cover information is important. In recent times, because of the expeditious urban growth, land cover information has made greatly in and around cities [2] [3]. Moreover, construction land has become progressively short, and the nonagriculturalization of arable land has been drawn special attention. Hence, it has become progressively important to well-timed; precisely detect land use/cover for the sensible advancement and use of urban land resources in city areas [4].

A great number of aerial images understanding that comprehensive information of the land surfaces unfasten a novel approach for large-cover classification with the advancement of aerial sensors. For novel investigation areas, land-cover classification of aerial images is basically on the basis of the supervised learning algorithms that need a great many annotated samples. However, it is time-consuming or strenuous or even unfeasible to explained original land-cover kinds of new aerial images. The collecting samples' cost will be minimized if formerly labeled data can be reutilized to classify a new image [5]. Nevertheless, diverse image acquisition states such as different illumination, sensors, seasonality, and natural environments impact the distribution of spectral characteristics images with similar image-level labels although, with diverse sensors, positions and environments exhibit the differences in spectral distributions through gray histograms. Hence, classification models learned from determined formerly annotated aerial images every time rapidly lose their effectiveness on new aerial images apprehended by different image acquisition states.

For remote-sensing data, the technology of fusion advancements and application at diverse spatial-temporal resolutions offer an effectual algorithm and approach to concurrently obtain both high temporal and spatial resolution data. For instance such as the STAARCH [9], STITFM [11], STARFM [10], and the RASTARFM [9] presented the STARFM technique to imitate reflectance data using blending MODIS and Landsat data, and the testing outcomes shown the efficiency of the STARFM on the basis of the actual and simulated data. In addition, the STARFM technique has been extensively exploited for LULC monitoring and mapping.

In many studies, even though the STARFM has been shown efficiently, there are still a few restrictions. For instance, the predicted image quality based upon the geographic areas of interest. Focusing to resolve these restrictions, [10] proposed an ESTARFM that enhances the indigenous method exploiting the noticed reflectance tendency among two points in time, and spectral unmixing supposition. Additionally, the ESTARFM is slowly applied to an extensive range of applications [11]. Hence, it is a practical manner to extract LULC information from time series Landsat images exploiting spatial-temporal fusion algorithms.

In recent time, in heterogeneous areas, the OBIA [9] was shown it’s possible in image classification. At the present time, deep learning has attained substantial favorable results in land-cover classification lately as they have the ability to extract high-level discriminative feature portrayal for aerial images. It is significant to discover how to efficiently transfer knowledge from the source domain to the destination domain using DCNN in deep learning-based algorithms. On the basis of the algorithms exploited in deep learning, this deep learning algorithm is classified into four types: such as mapping based deep learning, instance-based deep learning, network-based deep learning and adversarial based deep learning. In recent years, while comparing with the other three kinds of algorithms, the adversarial-based deep learning algorithms have the benefits which required no other restrictions and a factor variety can effortlessly be integrated into the adversarial-based deep learning architectures that tend to it's developing rapidly advancement.

The main aim of this work is to present a new land cover classification approach which consists of 3 major phases such as, Feature Extraction, Segmentation, and Classification. At first, from the segmented image, the VI feature vectors such as NDVI, SR, and Kauth–Thomas Tasseled Cap are extracted that are subsequently used for classification by exploiting NN. In addition, CNN is used for direct image classification. The average of both the classification result states the classification of water and land area. As the most important contribution element, the number of hidden neurons of both CNN and NN is optimized using the proposed Enhanced-CSA method.

2. Literature Review

In 2018, Ziwei Deng et al [1] worked on LULC in fast-rising city areas has more and more based upon remote-sensing data at maximum spatial and temporal resolutions. Nevertheless, because of the influence of revisiting weather and periods, it was complicated to obtain adequate time-series images with maximum quality at both maximum spatial and temporal resolution from a similar sensor. Here, the temporal-spatial fusion model was utilized to MODIS blend and Landsat8 data and attain time-series Landsat 8 images. Subsequently, by exploiting an object-based classification algorithm land cover information was extracted.

In 2019, Wenqiang Xia et al [2] exploited SITS data in resource examinations and environmental monitoring. Nevertheless, three distinctiveness geographic objects such as spatiotemporal correlation, temporal-spatio heterogeneity, and scale characteristics cause huge issues in the analysis of SITS. When, conventional studies pay no attention to these characteristics, which lead to unacceptable SITS analysis outcomes such as land-cover change detection and classification. Aspiring at interactively measuring and stating these three features, this work presents a spatiotemporal cube technique and an ST-MRS algorithm in order to analyze SITS.

In 2019, Chunping Qiua et al [3] presented the LCZ method to present an interdisciplinary taxonomy for UHI investigations. Recently, the method had also become an initial point for the growth of superior-level products. Due to the LCZ classes be able to aid present a generalized considerate of urban structures and land utilizes. Hence, LCZ mapping can notionally help in developing an enhanced considerate of Spatio-temporal dynamics of cities on a global scale. Nevertheless, reliable LCZ maps were not so far obtainable worldwide. As a primary step to routine LCZ mapping, this paper concentrates on LCZ-derived land cover classification, by exploiting multi-seasonal Sentinel-2 images. Moreover, Re-ResNet architecture was proposed which had the capability of learning a joint spectral-spatial-temporal feature symbol in a unitized framework.

In 2019, Ruixi Zhu et al [4] presented a SCDAL model incorporating three elements, such as filtering out simple triplets, presented hard adversarial learning, and triplet loss with center loss. In the SCDAL model, a complexity measure was presented to get rid of simple triplets in the constraint of between-class dissimilarity and intra-class similarity and enhanced distinguish hard triplets. Subsequently, the filtered triplets were exploited to train an additional discriminative source feature extractor with the proposed hard triplet loss integrating the semi-hard triplet loss and the hardest triplet loss. Additionally, adversarial learning with center loss was presented to minimize the feature distribution bias amid the source and destination feature extractors.

In 2018, Sory I. Tourea et al [5] presented a remote sensing data and algorithms were dependable tools for monitoring and examining urban LCLU modify. Moreover, FRe's commercial satellite image in combination with the GEOBICA algorithm was exploited to produce comprehensive and precise urban LCLU maps. The combination of a backdating algorithm enhances LCLU change classification outcomes for the initial date of a bi-temporal image series. On the other hand, modest spatial resolution satellite images like those from Landsat sensors might not let for detailed urban LCLU mapping. The main contribution of this paper was to test a novel bi-temporal change identification algorithm.

In 2018, Patrick Helber et al [6] presented a patch-based LCLU classification method by exploiting Sentinel-2 satellite images. It was explicitly and generously available and was proposed in the earth surveillance plan Copernicus. A new dataset was presented, on the basis of these images, which covers 13 spectral bands and was included of 10 classes with a total of 27000 labeled and geo-referenced images. Moreover, benchmarks were presented for this new dataset with its spectral bands by exploiting modern DCNN.

In 2019, Remi Ratajczak et al [7], created a novel multiscale multi-date dataset that included 4.9 million non-overlapping annotated patches of the France territory between 1970 and 1990 with the aid of Geography experts. Moreover, this dataset has been called as HistAerial. Subsequently, a widespread evaluation analysis of modern texture features classification and extraction techniques such as deep DCNNs was done and it was proposed in the form of an assessment. Finally, a new low-dimensional local texture filter called RCRLBP was proposed as an overview of the Binary Gradient Contours filter through the employ of an orthogonal amalgamation illustration.

In 2018, Corneliu Octavian Dumitru et al [8] presented the improved accessibility of high-resolution SAR satellite images that had to tend to novel civil technologies for the data. Among them, the methodical classification for land covers kinds on the basis of the patterns of settlements or agriculture recorded using SAR imagers.

3. Proposed Outline of Land Cover Classification

3.1 Proposed Architype

Consider the land cover image as $I = \{I_r, I_g, I_{nir1}, I_{nir2}\}$ that comprises of 4 bands such as green (I_g), red (I_r), and two NIR band (I_{nir1} and I_{nir2}). Here, two classifiers are exploited for classifying this image. At first, manually the 4 bands of the images are segmented and proposed to the NN classifier. For feature extraction and classification, the 4 band images are directly presented to CNN at the same time. Moreover, both the classifiers are exploited on account of CNN it has the ability to use the image directly and classify it on its own. Nevertheless, directly NN does not have the ability to access image, hence that based on the features of water and land, features are segmented and presented to NN for feature classification and extraction.

In feature extraction process, VI features are extracted and considered, such as (a) SR, (b) NDVI and (c) Kauth-Thomas Tasseled Cap. Eventually, to obtain a precise classified result; the average of both classified results is used. The precise result classified upshot exhibited whether the area is water or land. The result of the classifiers will be the labels that possess a close similarity to the classification of water and land. For that reason, the classified result of NN is indicated as O_{NN}, and the classified result of CNN is indicated as O_{CNN}. By exploiting an enhanced GWO algorithm named EGWO, the number of hidden neurons of both CNN and NN are optimized. The major contribution of this algorithm is to raise the classification precise. Subsequent to the classification, the average of two sets of labels is used by two classifiers, and it is contemplated as the concluding classification result. This result can classify if the concerned area of the image depends on land or water. In general, the diagrammatic demonstration of the proposed method is shown in Fig. 1.

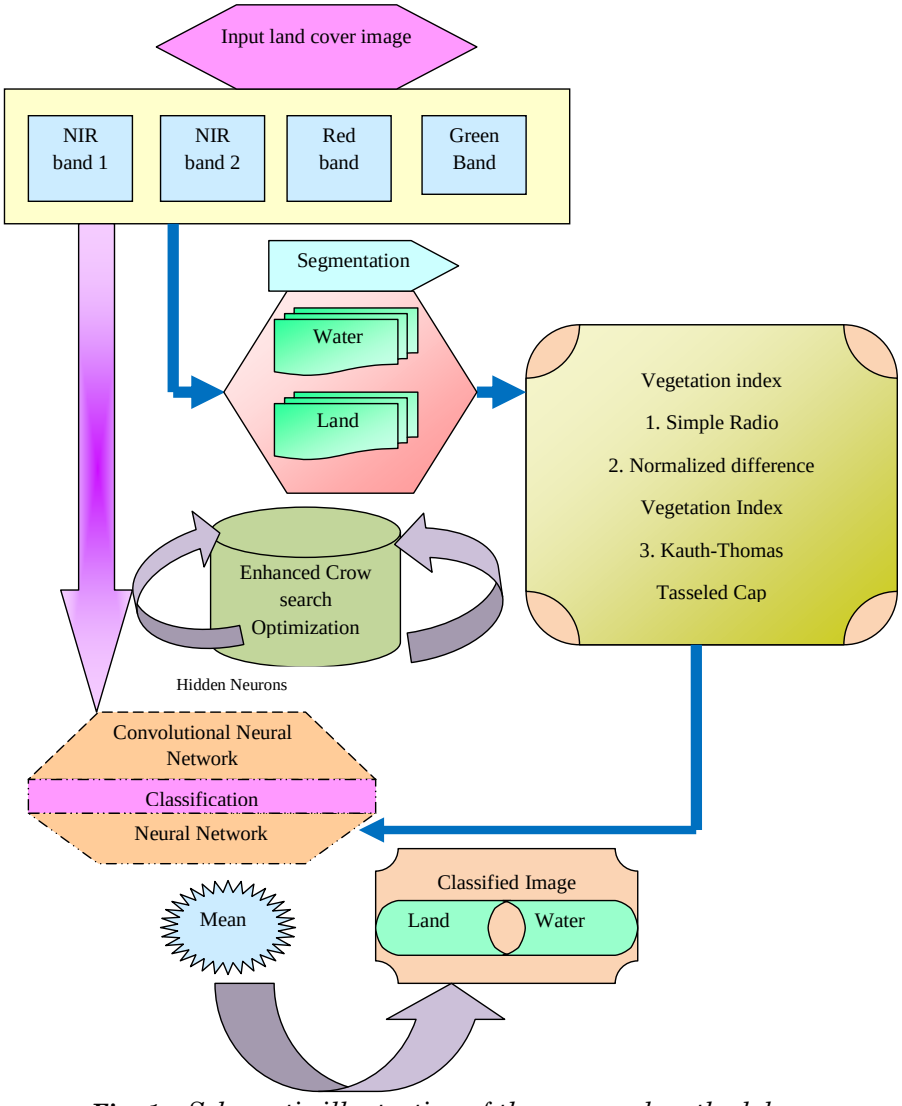

Fig. 1. *Schematic illustration of the proposed methodology*

3.2 Feature Extraction

The segmented image $I_{sm} \rightarrow \{I_{wr}, I_{lr}\}$ (I_{lr} represents the land area and I_{wr} represents water area) caused experience to feature extraction, to extract the features and to feature classification, the NN is used. Moreover, the VI feature vectors engage NDVI, SR, and Kauth-Thomas Tasseled Cap.

(i) SR: SR [15] is the easiest VI that is a ratio among the reflectance recorded in the Red and NIR bands. Additionally, it is mentioned that RVI indicates the number of vegetation directly. Using eq. (1), the SR is portrayed by the relation that RB denotes the red band of the image and nir indicates the close by an infrared band of the image.

$$SR = \frac{nir}{RB} \tag{1}$$

(ii) NDVI: NDVI is an easy portrayal measuring which can be exploited to verify remote sensing measurements, basically, however not certainly, from a space platform, and evaluates even if the target being seen comprises live green vegetation or not. In [15], it is observed as the easiest VI's which removes the topographic effects and the sun brightness angle, and the eq. (2) portrays the NDVI.

$$NDVI = \frac{(nir - RB)}{(nir + RB)} \tag{2}$$

(c) Kauth-Thomas Tasseled Cap: It is considered as the accessible technique for enhancing the spectral knowledge of data. For vegetation analysis, it specifically optimizes the screening of data. From the information of related six TM bands, the Tasseled Cap index is analyzed, in that three are most frequently used.

(i) Band 1 (a measure of brightness, soil)

(ii) Band 2 (a measure of greenness, vegetation)

(iii) Band 3 (interrelationship of soil wetness and canopy moisture)

Hence the extracted features are denoted using EF, which are subsequently offered to the NN classifier for classification process.

3.3 Classification based on Neural Network

For initial classification purposes, the extracted features EF are presented to the NN classifier. As stated in eq. (3), NN [16] [25] is a classifier that absorbs the features as the input, which nf indicates the number of features.

$$EF = \{EF_1, EF_2, ...EF_{nf}\} \tag{3}$$

As the NN comprises of the input layer, hidden layer, and output layer, it is a prerequisite to deciding the output of the hidden layer before calculating the complete network output. On the basis of eq. (4), the hidden layer output hl is decided, af denotes the activation function, i states the hidden neuron, j states the input neurons, n_i states the number of input neurons, w_i^G states the weight from j^{th} input neuron to i^{th} hidden neurons, w_{bi}^{Gi} states the bias weight to i^{th} hidden neuron, and F_i states the input features. Furthermore, the complete network output $\hat{H}_m$ is decided from the output layer that is exhibited in eq. (5), m states the output neurons, $w_{(im)}^{(H)}$ states the weight from i^{th} hidden neurons to m^{th} output neurons, n_h states the number of hidden neurons, and $w_{(Bm)}^{(H)}$ states the bias weight to m^{th} output neurons. As stated in eq. (5), the error among the actual and predicted values is computed that needs to be reduced. As stated in eq. (6), H_m states the actual output, n_H states the number of output neurons and $\hat{H}_m$ states the predicted output.

$$hl = af\left(w_{bi} + \sum_{j=1}^{n_i} w_{ji} F_i \right) \tag{4}$$

$$\hat{H}_m = af\left(w_{(Bm)}^{(H)} + \sum_{i=1}^{n_h} W_{(im)}^{(G)} hl_i \right) \tag{5}$$

$$ER^* = \underset{\left\{w_{(Bi)}^{(G)}, w_{(ji)}^{(G)}, w_{(Bm)}^{(H)}, w_{(im)}^{(H)}\right\}}{\arg\min} \sum_{m=1}^{n_G} \left| H_m - \hat{H}_m \right| \tag{6}$$

For reducing the error, the weight $w_1 = \left\{w_{(Bi)}^{(G)}, w_{(Bm)}^{(H)}, w_{(ji)}^{(G)}, w_{(im)}^{(H)}\right\}$ has to be tuned appropriately, which is performed using the proposed land cover classification. Hence, the output of classified features F_i is indicated O_{NN}.

3.4 Classification on the basis of the CNN

For the second classification, the land cover image I is presented to the CNN model. CNN exploits the spatial data between the pixels of an image and therefore, they are based upon discrete convolution. The basic elements of CNN are shown in [12] and [13]. Moreover, a grayscale image is presumed, which needs to be stated using a function as stated in eq. (7), so that image I can be identified by an array size of $a_1 \times a_2$[17].

$$I : \{1,...a_1\} \times \{1,...a_2\} \to P \subseteq \Re, (i,j) \mapsto I_{i,j} \tag{7}$$

Here for the image I, suppose filter $fl \in \Re^{2h_1+1 \times 2h_2+1}$, the discrete convolution with filter fl is denoted using eq. (8), in that filter fl is denoted using eq. (9).

$$(I * fl)_{p,s} := \sum_{v=-h_1}^{h_1} \sum_{u=-h_2}^{h_2} fl_{v,u} I_{p+v,s+u} \tag{8}$$

$$fl = \begin{pmatrix} fl_{-h_1,-h_2} & \cdots & fl_{-h_1,-h_2} \\ \vdots & fl_{0,0} & \vdots \\ fl_{h_1,-h_2} & .... & fl_{h_1,h_2} \end{pmatrix} \tag{9}$$

A usually exploited filter is the discrete Gaussian filter $fl_{G(\eta)}$[14], which is used for smoothing, exhibited using eq. (10), in that η states the S.D of Gaussian distribution.

$$\left(fl_{G(\eta)}\right)_{p,r} = \frac{1}{\sqrt{2\pi\eta^2}} \exp\left(\frac{p^2+s^2}{2\eta^2}\right) \tag{10}$$

Suppose layer r as a convolution layer, from a preceding layer in that input, comprises $n_1^{(r-1)}$ feature maps, with a size of $n_2^{(r-1)} \times n_3^{(r-1)}$. If r is 1, the input will be a single image I that affects 1 or more channels. Hence, CNN considers unprocessed images as input directly.

With size, $n_2^{(r)} \times n_3^{(r)}$ the output layer r consists of $n_1^{(r)}$ feature maps. In layer r, the i^{th} feature map denoted as $X_i^{(r)}$ and it is stated using eq. (11), in that, $C_i^{(r)}$ indicated bias matrix and $fl_{i,j}^{(r)}$ denotes the filter size of $2h_1^{(r)}+1 \times 2h_2^{(r)}+1$ which relates the i^{th} feature map in layer r with j^{th} feature map in layer $(r-1)$ [13].

$$Y_i^{(r)} = C_i^{(r)} + \sum_{j=1}^{n_1^{r-1}} fl_{i,j}^{(r)} * Y_j^{(r-1)} \tag{11}$$

As stated before, border effects affect $n_2^{(r)}$ and $n_3^{(r)}$. By using the discrete convolution in the valid segment of input feature maps that is for pixels in that summation of eq. (8) is showed precisely, the output feature maps comprise a size as exhibited in eq. (12).

$$n_2^{(r)} = n_2^{(r-1)} - 2h_1^{(r)} \text{ and } n_3^{(r)} = n_3^{(r-1)} - 2h_2^{(r)} \tag{12}$$

The eq. (13) states the linking of the convolutional layer and its function to a multilayer perceptron, and it can be rephrased. In layer r, each $Y_i^{(r)}$ comprises $n_2^{(r)}.n_3^{(r)}$ units arranged in a two-dimensional array. The eq. (14) exhibits the output, attained as an outcome of calculation by the unit at location (p,s).

$$\left(Y_i^{(r)}\right)_{p,s} = \left(C_i^{(r)}\right)_{p,s} + \sum_{j=1}^{n_1^{(r-1)}} \left(fl_{i,j}^{(r)} * Y_j^{(r-1)}\right)_{p,s} \tag{13}$$

$$\left(C_i^{(r)}\right)_{p,s} + \sum_{j=1}^{n_1^{(s-1)}} \sum_{v=-g_1^s}^{g_1^s} \sum_{u=-g_2^s}^{g_2^s} \left(fl_{i,j}^{(r)}\right)_{v,u} \left(fl_{i,j}^{(r)}\right)_{p,s} \left(Y_j^{(r-1)}\right)_{p+v,s+u} \tag{14}$$

In the bias matrices $C_i^{(r)}$ and filters $fl_{i,j}^{(r)}$, the trainable weights available in the network can be decided. Hence, the output of classified land cover image I is indicated as O_{CNN}.

3.5 Classified Labels

The obtained output classified labels from CNN, and NN indicated by O_{NN} and O_{CNN}, correspondingly is exploited, and do the average operation. The average of both the labels is represented as the last result that will be one or two, i.e. two states the water image and one states the land image.

4. Using Proposed Methodology Optimizing Number of Hidden Neurons

4.1 Objective Function

In this paper, the main contribution is to optimize or tune the number of hidden neurons of both NN and CNN classifiers. The hidden neurons of NN and CNN classifiers are subjected as input for solution encoding, whereas, $O_{NN} \rightarrow n_g$ indicates the total number of hidden neurons available in NN and O_{CNN} indicates the total number of hidden neurons available on CNN. The lower, and upper bound of O_{CNN} is (1,1,1), and (10,10,10), and O_{NN} is (1,1,1), and (25,25,25), correspondingly.

The main aim of the proposed land cover classification model is to increase the precision as stated in eq. (15), in that A_c states the classification accuracy as stated in eq. (16).

$$f_n = \min\left(\frac{1}{A_c}\right) \tag{15}$$

$$A_c = \frac{T_P + T_N}{T_P + T_N + F_P + F_N} \tag{16}$$

4.2 Enhanced CSA

In NN and CNN, the number of hidden neurons is optimized by using the proposed E-CSA technique. The Crow Search Algorithm has shown it's possible to discover the best solution for definite search spaces configurations [17]. However, its convergence is not assured because of its unsuccessful exploration of its search scheme. In this state, its search scheme states huge concerns while it faces high multi-modal formulations. In the conventional CSA algorithm, two dissimilar elements are primarily in charge of the search process such as the AP and the arbitrary movement (evasion). The AP value is in charge to present the balance among intensification and diversification. Conversely, directly the arbitrary movement affects the exploration process by the re-initialization of candidate solutions. In the proposed enhanced algorithm, both elements, the AP and the random movement, are reconsidered.

(a) DAP:

At the initial stage of the conventional CSA algorithm, the parameter AP is selected and remnants fixed in the optimization process. This detail is not favourable to the ratio of intensification and diversification. To enhance this relation, the AP is substituted by a DAP that is a probability value altered using the fitness quality of every candidate solution. The employ of probability parameters on the basis of the fitness values is effectively used in the evolutionary method [18]. Hence, the dynamic DAP is computed as stated below:

$$DAP_{i,j} = 0.9 \cdot \frac{F(Y_{i,j})}{\varpi U} + 0.1 \tag{17}$$

In eq. (17) ϖU indicates the worst fitness value observed hitherto. Presumptuous a reduction issue, this value is computed as follows $\varpi U = \max(F(Y_{k,j}))$. In this probabilistic method, promise solutions will encompass a maximum probability to be used. Conversely, solutions of bad quality will encompass a maximum probability to be re-initialized with a random location.

(b) Random Movement-Levy Flight:

The conventional CSA imitates two different behaviors of crows such as evasion and pursuit. The evasion behavior is imitated by the functioning of an arbitrary movement that is calculated by an arbitrary value uniformly distributed.

Naturally, the exploit of schemes to discover food is necessary to survive. A search algorithm that is not capable to search for better sources of food might be fatal for the animal. Lévy flights [19], is a kind of random walk that has been seen in many species as a foraging pattern.

In Levy flights, the step size is controlled by a heavy-tailed probability distribution generally called Levy distribution. Levy Flights are high competent than the uniform random distribution by exploring the search space [43].

In the proposed algorithm, with aspire to have a superior diversification on the search space, Levy flights are exploited rather than uniform arbitrary movements to imitate the behavior of evasion. Hence, a novel arbitrary location $F(Y_{i,j+1})$ is produced adding up to the present location $Y_{i,k}$ the calculated LF.

To attain a symmetric Levy stable distribution for LF the Mantegna method [20] is exploited. In the Mantegna algorithm, the initial phase is to compute the step size S_i as eq. (18).

$$S_i = \frac{c}{|d|^{1/\beta}} \tag{18}$$

In eq. (18), c and d represents n-dimensional vectors and $\beta = 3/2$. From the normal distribution, the elements of each vector c and d are sampled, which are represented by using eq. (19).

$$c \approx N(0, \eta_c^2) \qquad d \approx N(\eta_c^2)$$

$$\eta_c = \left\{ \frac{\Gamma(1+\beta)\sin(\pi\beta/2)}{\Gamma[(1+\beta)]\beta 2^{(\beta-1)/2}} \right\}^{1/\beta}, \quad \eta_c = 1 \tag{19}$$

Eq.(19) $\Gamma(\cdot)$ indicates a Gamma distribution. Subsequent to attaining the value of S_i, the factor LF is using eq. (20).

$$LF = 0.01 - S_i \circ (Y_{i,j} - Y^{best}) \tag{20}$$

In eq. (20), the product $\circ$ indicates the element-wise multiplications, Y^{best} indicates the optimal solution observed hitherto regarding the fitness quality. At last, the new location $Y_{i,j+1}$ is stated in eq. (21). Fig 2 shows the flow chart of the proposed E-CSA algorithm.

$$Y_{i,j+1} = Y_{i,j} + LF \tag{21}$$

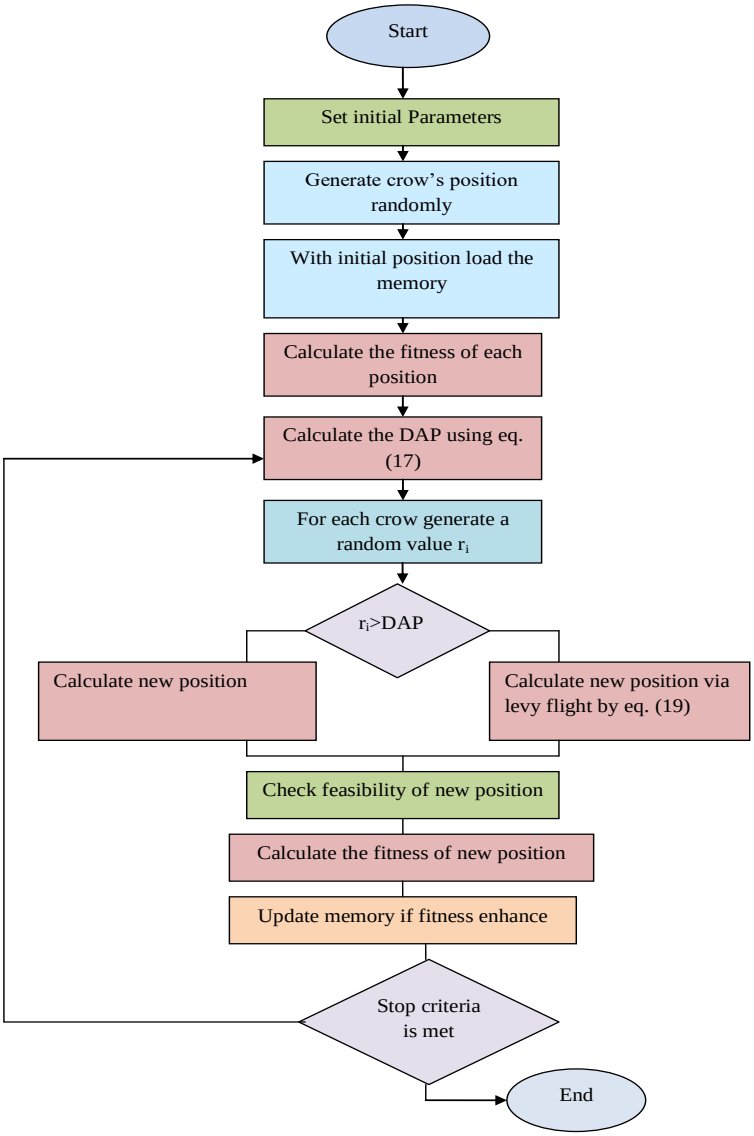

Fig. 2. *Flowchart of the proposed E-CSA algorithm*

5. Results and Discussions

5.1 Experimental Setup

The proposed land cover classification method was implemented in MATLAB 2018a, and the important outcomes were attained. The dataset was downloaded from the link, (https://earthexplorer.usgs. gov/: Access date: 2018-10-24. To the subsequently level of the performance, the proposed algorithm was evaluated with the existing methods such as, PSO−CNN+NN [22], ABC−CNN+NN [21], FF−CNN+NN [23], and GA−CNN+NN [24] methods regarding the performance measures namely accuracy, sensitivity, precision, specificity, FPR, FDR, NPV, FNR, F1- score and MCC. Additionally, the effect of learning percentage on the performance measures was also evaluated and the proposed E-CSA method obtained superior results. Moreover, 3 sample images with segmented images of the land cover classification method.

5.2 Performance Analysis

Fig 3 summarizes the graphical representation of land cover images for the proposed model with the conventional models regarding the performance measures namely accuracy, sensitivity, precision, specificity, NPV, FDR, FPR, FNR, F1- score and MCC. For accuracy measures, the proposed model is 31% outperforms the ABC-CNN-NN, 33% outperforms the PSO-CNN-NN, 44% outperforms the GA-CNN-NN, and 24% outperforms the FF-CNN-NN.

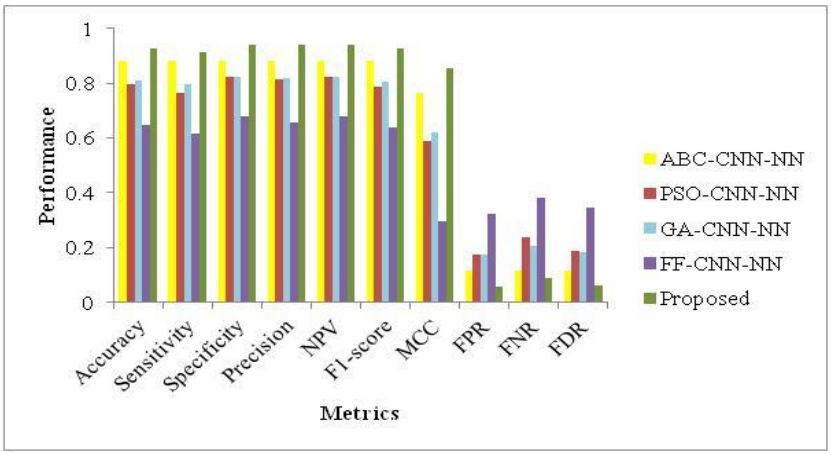

Fig. 3. *Graphical representation of land cover images*

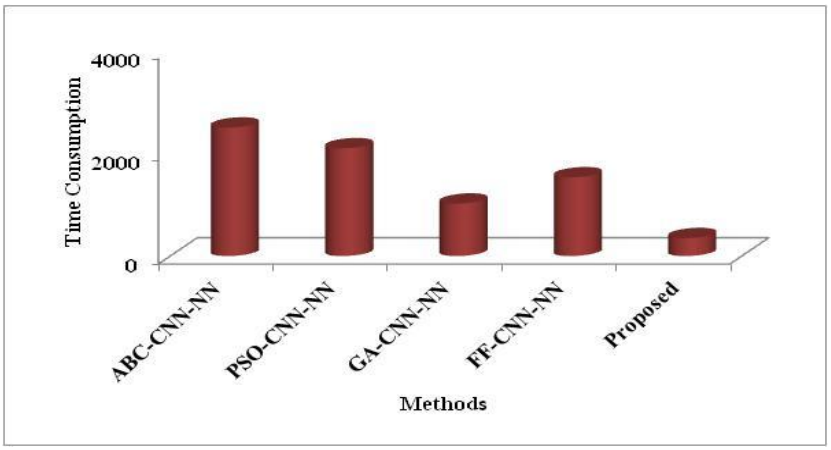

Fig. 4. *Graphical representation of Computational Complexity*

Fig 4 demonstrates the graphical representation of computational complexity for the proposed model with the conventional models. Here, the proposed model is 15% outperforms the ABC-CNN-NN, 17% outperforms the PSO-CNN-NN, 21% outperforms the GA-CNN-NN, and 27% outperforms the FF-CNN-NN.

6. Conclusion

In this paper, a new land cover classification approach was proposed that consists of three important phases like segmentation, feature classification and extraction. First and foremost, the land cover image was segmented and it was proposed for the feature extraction process. At feature extraction, VI like, NDVI, SR, and Kauth–Thomas Tasseled Cap was extracted, that were given to classification by exploiting NN. Moreover, using CNN the image was directly classified. As an innovation, the hidden neurons of both NN and CNN were optimized using the proposed E-CSA. The hidden neurons were optimized so that the classification precision has to be immense. From averaging the CNN and NN result, the final result of classification was attained. Moreover, the proposed E-CSA method was well-known with conventional methods, and the results were evaluated.

References

[1] Ziwei Deng, Xiang Zhu, Qingyun He, Lisha Tang,"Land use/land cover classification using time series Landsat 8 images in a heavily urbanized area",Advances in Space Research, Volume 63, Issue 7, 1 April 2019, Pages 2144-2154.

[2] Wenqiang Xi, Shihong Du, Yi-Chen Wang, Xiuyuan Zhang,"A spatiotemporal cube model for analyzing satellite image time series: Application to land-cover mapping and change detection", Remote Sensing of Environment, Volume 231, 15 September 2019.

[3] Chunping Qiu, Lichao Mou, Michael Schmitt, Xiao Xiang Zhu,"Local climate zone-based urban land cover classification from multi-seasonal Sentinel-2 images with a recurrent residual network", ISPRS Journal of Photogrammetry and Remote Sensing, Volume 154, August 2019, Pages 151-162.

[4] Ruixi Zhu, Li Yan, Nan Mo, Yi Liu," Semi-supervised center-based discriminative adversarial learning for cross-domain scene-level land-cover classification of aerial images" ISPRS Journal of Photogrammetry and Remote Sensing, Volume 155, September 2019, Pages 72-89.

[5] Sory I. Toure, Douglas A. Stow, Hsiao-chien Shih, John Weeks, David Lopez-Carr,"Land cover and land use change analysis using multi-spatial resolution data and object-based image analysis" Remote Sensing of Environment, Volume 210, 1 June 2018, Pages 259-268.

[6] P. Helber, B. Bischke, A. Dengel and D. Borth, "EuroSAT: A Novel Dataset and Deep Learning Benchmark for Land Use and Land Cover Classification," IEEE Journal of Selected Topics in Applied Earth Observations and Remote Sensing, vol. 12, no. 7, pp. 2217-2226, July 2019.

[7] R. Ratajczak, C. F. Crispim-Junior, E. Faure, B. Fervers and L. Tougne, "Automatic Land Cover Reconstruction From Historical Aerial Images: An Evaluation of Features Extraction and Classification Algorithms," IEEE Transactions on Image Processing, vol. 28, no. 7, pp. 3357-3371, July 2019.

[8] C. O. Dumitru, G. Schwarz and M. Datcu, "SAR Image Land Cover Datasets for Classification Benchmarking of Temporal Changes," IEEE Journal of Selected Topics in Applied Earth Observations and Remote Sensing, vol. 11, no. 5, pp. 1571-1592, May 2018.

[9] Gao, F., Masek, J., Schwaller, M., Hall, F., 2006. On the blending of the landsat and modis surface reflectance: predicting daily landsat surface reflectance. IEEE Trans. Geosci. Remote Sens. 44 (8), 2207–2218.

[10] Hilker, T., Wulderb, M.A., Coopsa, N.C., 2009. A new data fusion model for high spatial- and temporal-resolution mapping of forest disturbance based on landsat and modis. Remote Sens. Environ. 113 (8), 1613–1627.

[11] Wu,M.Q., Niu, Z., Wang, C., Wu, C., Wang, L., 2012. Use of MODIS and Landsat time series data to generate high-resolution temporal synthetic Landsat data using a spatial and temporal reflectance fusion model. J. Appl. Rem. Sens. 6, 063507.

[12] Mohan Y, Chee SS, Xin DKP, et al. Artificial neural network for classification of depressive and normal in EEG. 2016 IEEE EMBS Conference on Biomedical Engineering and Sciences (IECBES), 2016.

[13] Jarrett K, Kavukcuogl K, Ranzato M, et al. What is the best multi-stage architecture for object recognition? In Computer Vision, International Conference on, 2009, p. 2146–2153.

[14] LeCun Y, Kavukvuoglu K, Farabet C. Convolutional networks and applications in vision. In Circuits and Systems, International Symposium on, 2010, p. 253–256.

[15] Forsyth D, Ponce J. Computer vision: a modern approach. New Jersey: Prentice Hall Professional Technical Reference; 2002.

[16] Zheng Y-J. Water wave optimization: a new nature-inspired metaheuristic.Comput Oper Res. 2015 Mar;55:1–11.

[17] Askarzadeh, A. A novel metaheuristic method for solving constrained engineering optimization problems: Crow search algorithm. Comput. Struct. 2016, 169, 1–12.

[18] Karaboga, D.; Basturk, B. A powerful and efficient algorithm for numerical function optimization: Artificial bee colony (ABC) algorithm. J. Glob. Optim. 2007, 39, 459–471.

[19] Baronchelli, A.; Radicchi, F. Lévy flights in human behavior and cognition. Chaos Solitons Fractals 2013, 56, 101–105.

[20] Yang, X.-S. Nature-Inspired Metaheuristic Algorithms; Luniver Press: Beckington, UK, 2010.

[21] Kıran MS, Fındık O. A directed artificial bee colony algorithm. Appl Soft Comput. 2015 Jan;26:454–462.

[22] Zhang J, Xia P. An improved PSO algorithm for parameter identificationof nonlinear dynamic hysteretic models. J Sound Vib. 2017 Feb;389:153–167.
[23] Fister I, Fister I,Yang X-S, et al.Acomprehensive reviewof firefly algorithms. Swarm Evol Comput. 2013 Dec;13:34–46.
[24] McCall J. Genetic algorithms for modelling and optimisation. J Comput Appl Math. 2005 Dec;184(1):205–222.
[25] Arul.V.H,V.G.Sivakumar,Ramalatha Marimuthu and Basabi Chakraborty,"An Approach for Speech Enhancement Using Deep Convolutional Neural Network",Multimedia Research, Volume 2, Issue 1, Januray 2019.